Available online at www.eccomasproceedia.org
Eccomas Proceedia COMPDYN (2025) 139-154

ECCOMAS
Proceedia

COMPDYN 2025
10th ECCOMAS Thematic Conference on
Computational Methods in Structural Dynamics and Earthquake Engineering
M. Papadrakakis, M. Fragiadakis (eds.)
Rhodes Island, Greece, 15-18 June 2025

A NEW HOURGLASS LATTICE TRANSITION PIECE TO MITIGATE THE SEISMIC RESPONSE OF OFFSHORE WIND TURBINES

Yucheng Peng[1] **and Alessandro Tombari**[2]

[1] University of Exeter
North Park Road Exeter UK EX4 4QF
e-mail: yp307@exeter.ac.uk

[2] University of Exeter
a.tombari@exeter.ac.uk

Abstract

Wind turbines are slender, lightly damped structures, making them particularly susceptible to earthquake-induced vibrations. With the ongoing expansion of wind energy into new markets, where taller and larger turbines are being installed in seismically active regions, seismic design has become a critical consideration. Historically, seismic effects have often been overlooked in the design of smaller turbines, but in certain regions, earthquake-induced vibrations may dominate over wind or wave-induced loads. Effective mitigation of seismic responses is hence essential to enhance structural reliability and safety.

This paper introduces a novel seismic mitigation strategy by redesigning the traditional transition piece of bottom-fixed offshore wind turbines into a seismic device termed the Hourglass Lattice Transition Piece. This innovative design builds on the previously proposed Reduced Column Section to control and reduce stress concentrations in the tower and monopile. The design has been further optimised to incorporate a lattice structure that enhances seismic performance by improving stress control, allowing an easier retrofitting of plasticised elements, and facilitating re-centring of permanent tilts induced by extreme events.

The proposed approach is validated through numerical analysis using the 15-megawatt reference turbine developed by the International Energy Agency. A 3D finite element model of the turbine is subjected to combined wind, wave, and seismic loadings to evaluate its dynamic response. The paper highlights the key features of the Hourglass Lattice Transition Piece, its simplified design methodology, and its benefits in enhancing the seismic resilience of wind turbines in earthquake-prone areas.

Keywords: Instructions, ECCOMAS Thematic Conference, Structural Dynamics, Earthquake Engineering, Proceedings.

ISSN:2623-3347 Published by Eccomas Proceedia.
Peer-review under responsibility of the organizing committee of COMPDYN 2025.
doi: 10.7712/120125.12398.25507

1 INTRODUCTION

Dedicated to providing clean and sustainable electricity, the offshore wind energy industry has seen dramatic development in the past decades, both technologically and commercially, where wind turbines have evolved from 5 MW to 15 MW and recently to 20 MW, while global total installed power capacity exceeded 1000 GW in 2023 [1]. As this prospering trend suggests, offshore wind turbines with higher rated-power capacity, consisting of larger blades and greater rotor altitude, are in the course of future [2]. Unexplored earthquake-prone regions will be on the list of potential wind farm sites [3], including the coastline of the United States, Japan, China, the Philippines and other countries. As a slender and flexible structure, the wind turbine is susceptible to earthquake-induced vibration. From the perspective of both ultimate limit state (ULS) and serviceability limit state (SLS) design, seismic activity becomes a crucial factor.

Researchers have performed studies to understand how wind turbines behave during earthquake. Offshore wind turbines with different supporting structures [4] were investigated in terms of seismic response, showing that monopile-supported OWT obtains the highest maximum horizontal displacement at the top of tower. Padrón et al., [5] analyzed the dynamic response of 5 MW, 10 MW and 15 MW offshore wind turbine under earthquake and concluded that soil-structure interaction plays an important role affecting the response of structure, while even low to moderate intensity ground motion can impact wind turbines significantly. Liang et al., [6] examined the wind-wave-seismic combined action on wind turbine with scoured site condition, where scour depth and soil type alter the dynamic response of the structure.

Therefore, proposing innovative solutions to mitigate the seismic response of wind turbines is of paramount importance. Vibration-control strategies for wind turbines are investigated by Lu et al., [7], who proposed a multi-tuned mass damper (MTMD) system to control the dynamic response under combined wind-wave-seismic loading and effectively reduce peak spectral values in frequency-domain analysis. Gao et al., [8] designed tuned mass dampers (TMDs) considering optimization and various load cases, and in-site implementation of TMDs indicates significant reduction in terms of side-side response. Ke et al., [9] developed a self-centering jacket-type offshore wind turbine by applying an energy dissipation bearing to the base of tower to improve structural fragility and serviceability.

In this study, a novel device called the Hourglass Lattice transition piece Structure (HLS) to replace the traditional transition piece is proposed. The HLS is based on the working principles of the Reduced Column Section (RCS) approach developed in [10-11] for wind-turbine vibration control. The study shows the effectiveness of the new HLS in mitigating the combined wind-seismic response of the IEA 15 MW reference wind turbine [12].

2 HOURGLASS LATTICE STRUCTURE

2.1 15 MW reference wind turbine model

The IEA 15 MW reference offshore wind turbine [12], which is schematically depicted in Figure 1a, is adopted in this study as the baseline model. A numerical finite element model is created in OpenSeesPY [13] using elastic Euler-Timoshenko beam elements for its main components, such as monopile, transition piece (TP) and tower segments. Additionally, the rotor-nacelle assembly (RNA) is modelled by two lumped masses, representing the rotor hub and nacelle, located in the space according to the actual eccentricity, as shown in Figure 1b, and linked to the top of the tower (TOT) through rigid link constraints

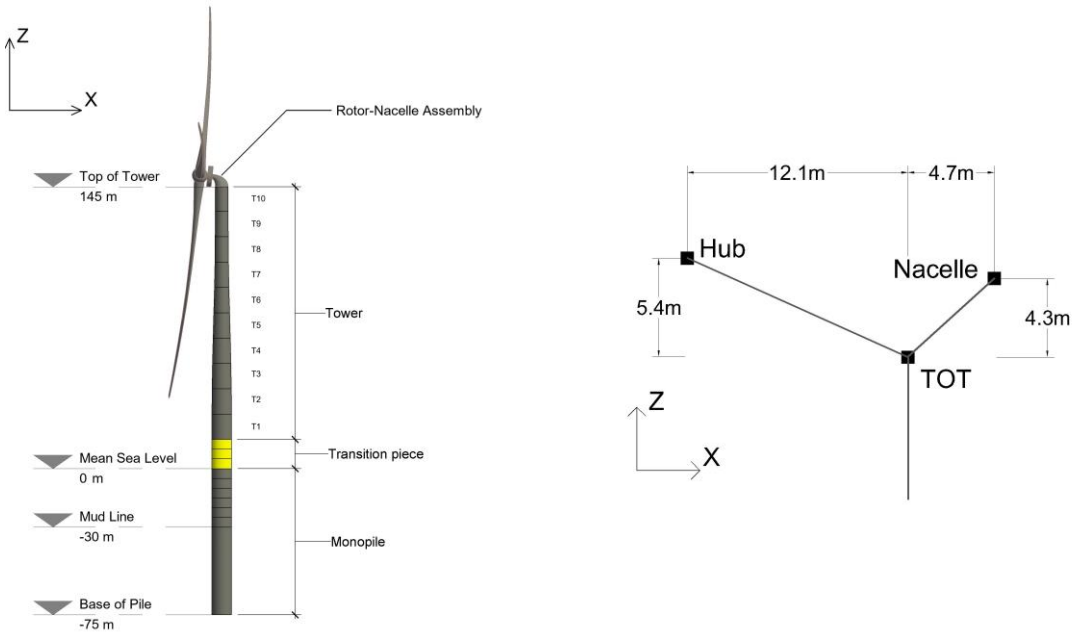

(a) (b)

Figure 1: (a) Elevation view of 15 MW reference offshore wind turbine and (b) Rigid link constraints depicting the rotor-nacelle assembly.

The material used for the wind turbine structure is a linear elastic steel, with a Young's Modulus of 210 GPa and a Poisson's ratio of 0.3. The reference wind turbine is founded on a homogeneous soil deposit characterised by Young's Modulus of 140 MPa and a Poisson's ratio of 0.4. Soil-pile interaction is captured through a series of distributed spring-dashpot systems along the monopile element, as depicted in Figure 2. Each unit consists of a two-joint link characterised by linear elastic springs with a constant stiffness and damping coefficient of 971600 kN/m and 17046 kN/ms, respectively. Additional restraints are applied to the pile toe to restrict translational motion about the vertical Z-direction and pile torsional behaviour.

2.2 Wind and seismic loading

The wind turbine model is subjected to a combined action of wind and seismic loading. The wind is modelled through aerodynamic forces computed using OpenFAST, where the mean wind speed is set to 10 m/s, which is close to the rated wind speed of the 15 MW wind turbine. A time history of 130 s duration is considered. The generated aerodynamic loads, applied to

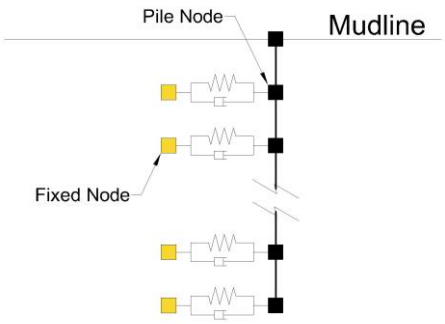

Figure 2: Schematic of the soil-pile interaction system.

the hub of the wind tower, comprise 6 components, namely, $F_{x,Wind}$, $F_{y,Wind}$, $F_{z,Wind}$, $M_{x,Wind}$, $M_{y,Wind}$ and $M_{z,Wind}$. The fore-aft force $F_{x,Wind}$ is depicted in Figure 3a.

The seismic load is defined as a series of X-direction displacement history functions, applied to the related soil springs at each horizontal level. The displacement time history functions are obtained through a linear site response analysis on the soil characterised by shear wave velocity of 265 m/s. The seismic event is representative of an abnormal level earthquake through the application of a multiplier factor of 1.6. In this study, the earthquake occurs after 100 seconds of wind loading, lasting 30 seconds. Its dynamic effects are superimposed on the aerodynamic loads acting on the wind turbine. Figure 3b shows the displacement time-history function at the mudline.

2.3 Hourglass lattice structure

In order to mitigate the combined action of wind and seismic loading, an alternative design of the traditional cylindrical TP, dubbed hourglass lattice transition (HLS), is herein proposed. The HLS is a space lattice truss which has been devised according to the working principles of the Reduced Column Section (RCS) approach [10-11]. The approach essentially aimed to generate a "weak" region to achieve the following objectives: i) fundamental period elongation (if consistent with the design option), ii) concentration of the maximum stresses in the RCS for protection of the remaining segments, and iii) hysteresis dissipation during extreme events. The HLS is devised to extend the above principles by adding features such as ease of element replacement, use of dissipating devices and advanced materials for boosting dissipation as well as self-recentring. Schematic views of the HLS are shown in Figure 4, where its lattice structural members are classified as columns, diagonal bracings, core bracings, lateral bracings, and spatially spanning bracings for maintaining stability.

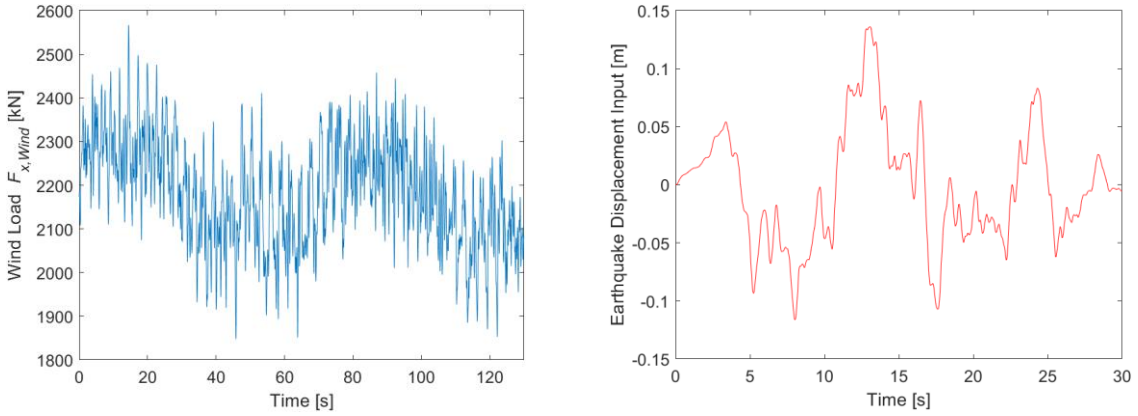

(a) (b)

Figure 3: (a) Wind load input at hub and (b) Seismic action input at mudline.

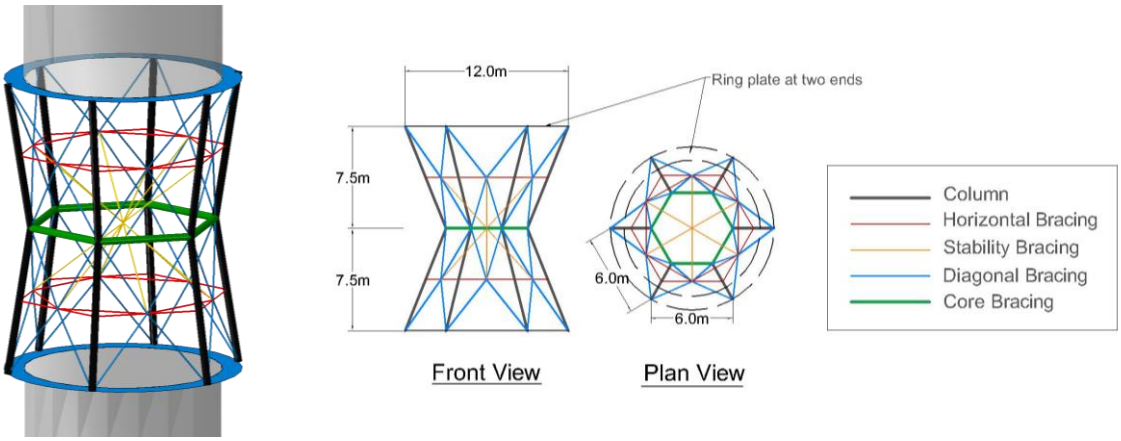

(a) (b)

Figure 4: (a) 3-dimensional view and (b) Schematic drawing of the HLS transition piece structure.

The diameter of the middle section is reduced to form an hourglass shape. Reduction ratio (RD) is determined based on the proportion of the circumradius at the core to the circumradius at the base (which is defined as 6 m). In this research, 2 reduction ratios are tested, namely, RD = 0.5, RD = 0.8 and additionally, a case with a larger section (RD = 1.1) is also considered. It is worth mentioning that although the reduction ratio can be greater than 1, the HLS principles can still be applied by proper design of the individual truss elements. Sketches of the three cases are illustrated in Figure 5.

The final design consists of a symmetric structure with horizontal layers placed in the middle between the core and the bases, where the connections with the tower and monopile are realised. Horizontal and stability bracings are then added at the layer to ensure stability. The HLS replaces the traditional transition piece of the considered IEA 15 MW Reference wind turbine [12], previously described. Therefore, the modelling of RNA, tower and monopile is unchanged. The numerical models are visualized in Figure 6a and Figure 6b, for reference and an HLS-protected wind turbine, respectively.

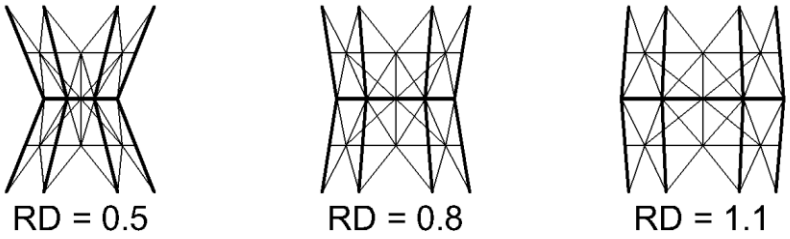

Figure 5: HLS at different reduction ratios.

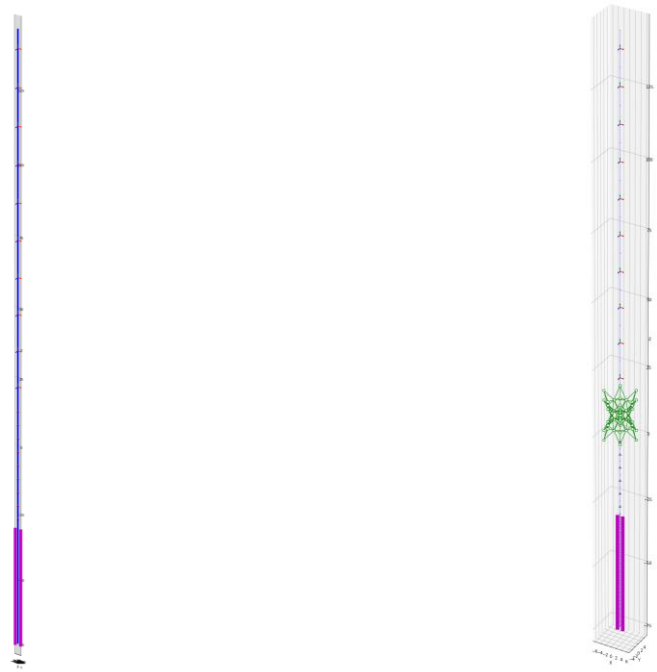

(a) (b)

Figure 6: Numerical wind turbine models with (a) traditional TP and (b) Hourglass Lattice Structure.

2.4 Optimisation of the HLS

In this section, the HLS is designed to mitigate the combined action of wind and seismic response of the IEA 15 MW reference wind turbine. The optimisation process aims to establish the optimal area of the columns, A_c, and the area of the diagonal bracings, defined as a ratio R_b with respect to A_c. The bending moment at the mudline, M_y, is used for defining the objective function of the optimisation process. A Differential Evolution (DE) algorithm [14] is used. The DE method is divided into 4 steps as follows:

1. **Initialization**: For a particular generation G, within the given bounds for A_c, $0.04\ \text{m}^2 \leq A_c \leq 0.3\ \text{m}^2$, and R_b, $0.05 \leq R_b \leq 0.6$, the algorithm first randomly creates a target vector (population), $\boldsymbol{x_G} = [x_{1,G}, x_{2,G}, \dots, x_{N_P,G}]$ where $\boldsymbol{x_{i,G}} = [A_c, R_{b,i}]$, and N_P is the population size set to 15 in this study. Each pair of values A_c and R_b are the candidate agents that will be used to perform the dynamic analysis of the wind turbine protected by HLS to compute the bending moment at the mudline, $M_{y,Ini}$.

2. **Mutation**: To increase the diversity of the population in the search-space, a mutant vector is then introduced based on the difference between candidate agents, where

$$\boldsymbol{v_{i,G+1}} = \boldsymbol{x_{r1,G}} + F \cdot \left(\boldsymbol{x_{r2,G}} - \boldsymbol{x_{r3,G}}\right) \tag{1}$$

   Here, $\boldsymbol{v_{i,G+1}}$ is the mutant vector, $\boldsymbol{x_{r1,G}}$, $\boldsymbol{x_{r2,G}}$ and $\boldsymbol{x_{r3,G}}$ are the candidate agents randomly chosen from the current population $\boldsymbol{x_G}$, while F denotes a stochastic scaling factor selected between 0.5 and 1.

3. **Recombination**: With the mutant vector, recombination (also called crossover) then is performed to form a trial vector $\boldsymbol{u_{i,G+1}} = [u_{1i,G+1}, u_{2i,G+1}, \dots, u_{Di,G+1}]$, in which D denotes the number of variables (here, $D = 2$). The components of the trial vector are determined by crossover probability and a random index; a detailed procedure is reported in [14] which highlights whether the components of the candidate agent $\boldsymbol{x_{i,G}}$ or the mutant vector $\boldsymbol{v_{i,G+1}}$ should be used to constitute the trial vector $\boldsymbol{u_{i,G+1}}$. Recombination

blends the mutant vector and target vector to form a new trial vector, introducing more diversity to the selection of A_c and R_b.

4. **Selection**: The pair of values (A_c and R_b) in $\boldsymbol{u_{i,G+1}}$ from recombination are then used to compute mudline moment $M_{y,Rec}$. If the trial vector $\boldsymbol{u_{i,G+1}}$ returns smaller M_y than the output of $\boldsymbol{x_{i,G}}$ ($M_{y,Ini}$), $\boldsymbol{u_{i,G+1}}$ will be retained as the candidate agent $\boldsymbol{x_{i,G+1}}$ for the next generation and vice versa. The maximum iteration number is set to 50 to limit computational expense while ensuring a sufficient number of iterations.
5. **Termination:** During the optimisation, the magnitude of M_y decreases, and the range of variables (A_c and R_b) for candidate agents narrows as the iteration continues. Once the standard deviation of the variable range is within the tolerance set to 0.01 in this study, the best result from the population $\boldsymbol{x_{final}}$ will be treated as the globally optimal result, and the optimisation algorithm stops.

The complete optimisation procedure is shown in Figure 7.

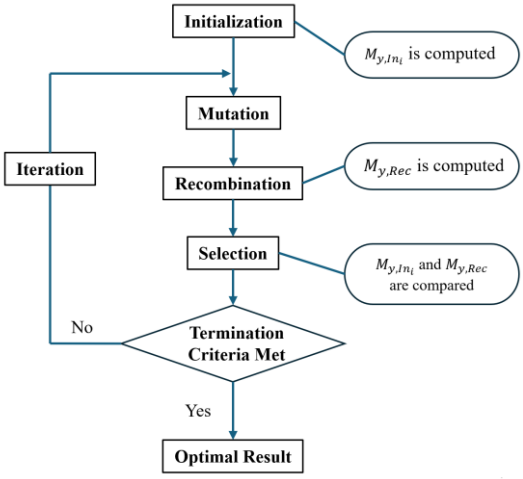

Figure 7: Flowchart of differential evolution optimisation.

3 RESULTS

3.1 Optimal geometry and frequency analysis

The global optimisation is performed to identify the optimal sections of columns, A_c, and diagonal bracings (where $A_{db} = A_c \times R_b$) for each investigated RD case. Regarding the remaining parameters, the area of core bracing is defined equal to the column's area, while the horizontal bracings and stability bracings' areas are kept constant. Geometrical parameters, including the computed optimal values, are presented in Table 1. A frequency analysis is also conducted to understand if the wind turbine equipped with the optimal HLS still falls in the soft-stiff region with a first frequency between the rotational frequency of rotor (1P) and the blade passing frequency of 3 bladed turbine (3P).

The 1P and 3P domains of the 15 MW wind turbine are 0.083-0.126 Hz and 0.249-0.378 Hz, respectively [12]. Based on the results shown in Table 2, the optimized HLS shift the wind turbine 1st natural frequency always between the soft-stiff region.

Case	Column	Diagonal Bracing	Core Bracing	Lateral Bracing	Stability Bracing
RD = 0.5	0.2305	0.0789	0.2305	0.0021	0.0021
RD = 0.8	0.1141	0.0057	0.1141	0.0021	0.0021
RD = 1.1	0.0450	0.0023	0.0450	0.0021	0.0021

Table 1: Optimal sectional area of truss members (m^2).

3.2 Verification

To ensure that the numerical models are properly capturing the complex wind-seismic response, a 3D shell model is also built in ABAQUS [15]. Compared to the beam model, the wind turbine tower, the reference cylindrical TP and monopile are modelled with 8-node shell elements to capture the behaviour of thin-walled structures. Mesh density is refined in the top half of the tower to better capture the peak local stresses and deformations. The HLS is modelled with 3-dimensional 2-node truss elements. The connections between the cylindrical TP and tower and monopile are defined as tie constraints, while kinematic coupling constraints are adopted to form the connections between HLS transition piece and other shell structures. Soil-pile interaction is modelled similarly to what is done for the beam model. Figure 8 shows the 3D wind turbine models used to verify the simplified beam models of Figure 6.

	Reference		RD = 0.5		RD = 0.8		RD = 1.1	
Mode	Fore-aft	Side-side	Fore-aft	Side-side	Fore-aft	Side-side	Fore-aft	Side-side
1	0.1620	0.1625	0.1457	0.1460	0.1435	0.1438	0.1400	0.1403
2	1.0377	1.0876	1.0115	1.0576	0.9943	1.0727	0.9366	0.9878
3	2.6814	3.1377	2.3963	2.6470	2.4889	2.8187	2.4067	2.7715
4	4.7528	6.1447	4.2035	5.2844	4.3368	5.3274	4.5951	5.3106
5	7.8094	10.1992	7.1388	9.7118	6.4895	7.8145	5.5041	6.6929
6	12.1680	15.2019	11.7770	13.9699	9.1892	11.3717	8.8079	11.8320

Table 2: Natural frequencies of reference and HLS wind turbines (Hz).

(a) (b) (c)

Figure 8: ABAQUS model of: (a) Reference, (b) RD = 0.8 and (c) RD = 1.1.

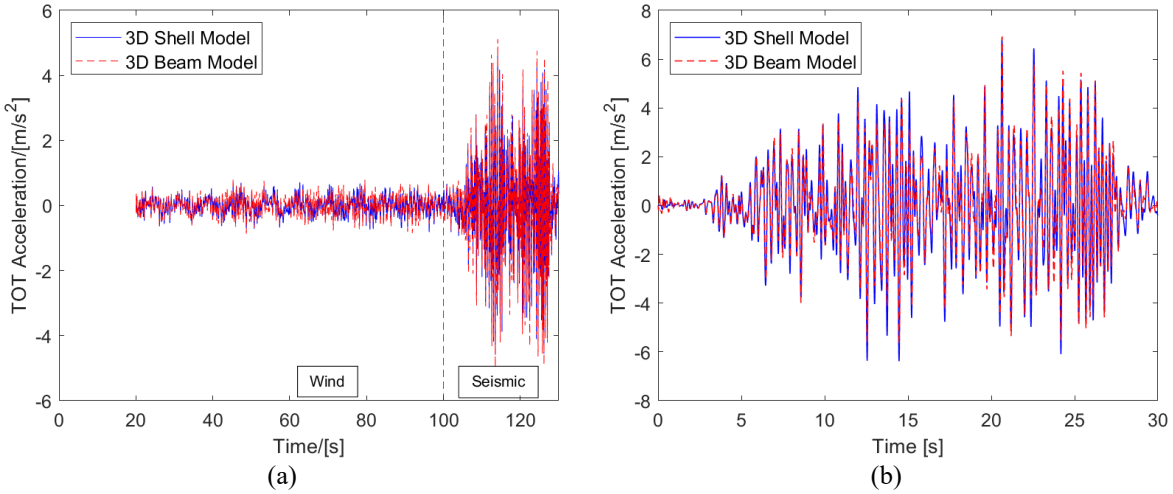

Figure 9: Acceleration time-history results between beam model and shell model: (a) Wind-seismic combined and (b) Seismic-only.

Two analyses are used for the model verification: a combined wind-seismic analysis as well as a seismic-only analysis. Results are shown in terms of acceleration in the X-direction at the top of tower (TOT). Figure 9a and Figure 9b shows the good agreement of the beam model with the more complex 3D shell model for combined action and seismic-only analysis, respectively.

3.3 Combined wind-seismic analysis

In this section, the benefits of using the HLS in mitigating the combined wind-seismic loading are evaluated. Figure 10 shows the bending moment envelope under the combined action of wind and earthquake. It is worth noting that since truss elements are applied to the HLS, no bending moment exists within the transition piece region.

It can be observed that for the case of RD = 1.1, the area of the bending moment envelope is significantly reduced, and the reduction is evident within the entire tower and monopile; 36% reduction in mudline bending moment and up to 40% reduction on the tower can be observed compared to the reference. Good results are also obtained for the case of RD = 0.8 with a reduction of 23% at the mudline and a maximum reduction of 26% on the tower. On the other hand, the bending moment at the top of the tower (segment T10) is 10% greater than the reference turbine, although this outcome can be improved by either changing the reduction factor or adding dissipative behaviour to the HLS.

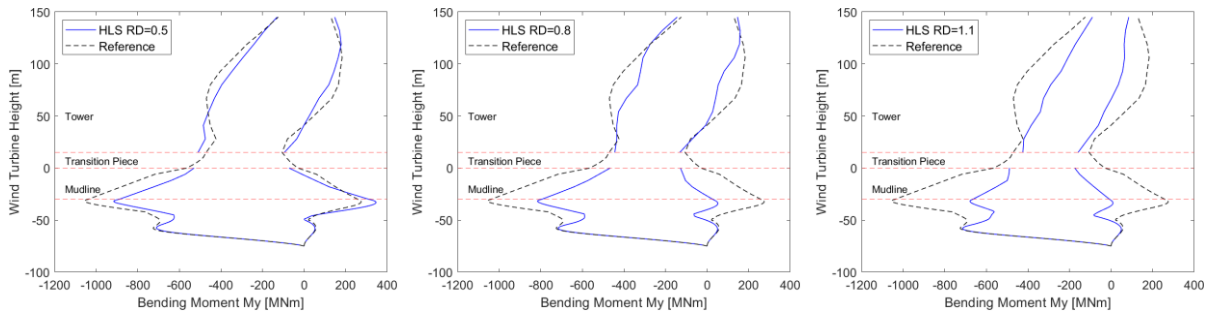

Figure 10: Bending moment envelope compared to the reference: (a) RD = 0.5, (b) RD = 0.8 and (c) RD = 1.1.

Lowest results are obtained for RD = 0.5 HLS wind turbine, where the bending moment at mudline decreases by 14%, and the response in the top-half of tower segments shows limited mitigation (10% on average). This can also be improved by changing the objective function and aiming to mitigate different regions than the monopile. Figure 11 illustrates the displacement and acceleration time histories of each HLS case compared to the baseline response. The reduction in peak acceleration value for RD = 1.1, RD = 0.8, and RD = 0.5, are 34.58%, 3.31% and 5.44%, respectively, suggesting that HLS transition piece also mitigates dynamic response in terms of acceleration, because of the shift in the fundamental period.

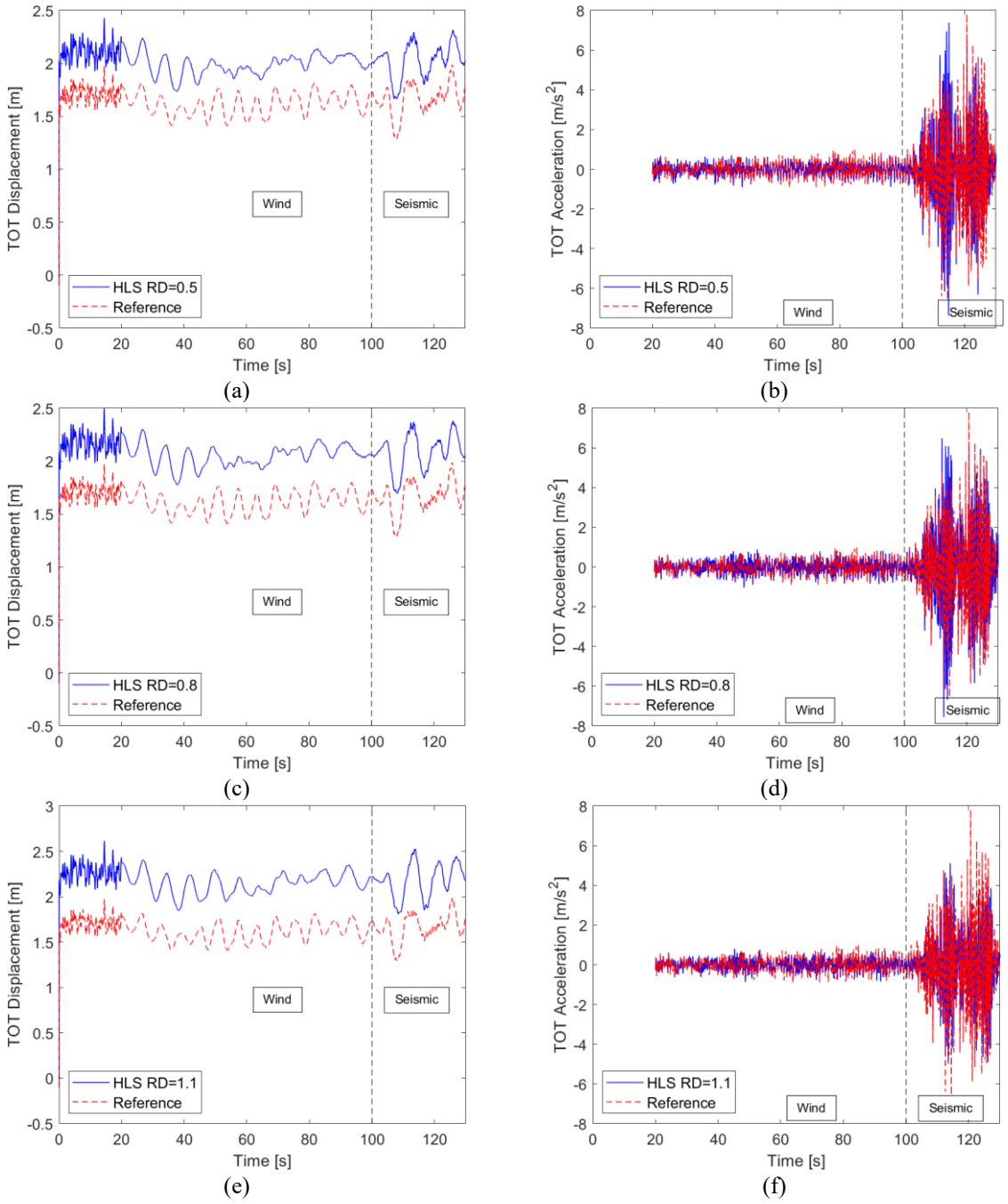

Figure 11: Displacement and acceleration compared to the reference: (a, b) RD = 0.5, (c, d) RD = 0.8, and (e, f) RD = 1.1.

Consistently, the HLS transition-piece supported wind turbines also experience greater horizontal displacements than the reference structure under wind loading, which should be controlled during the design phase.

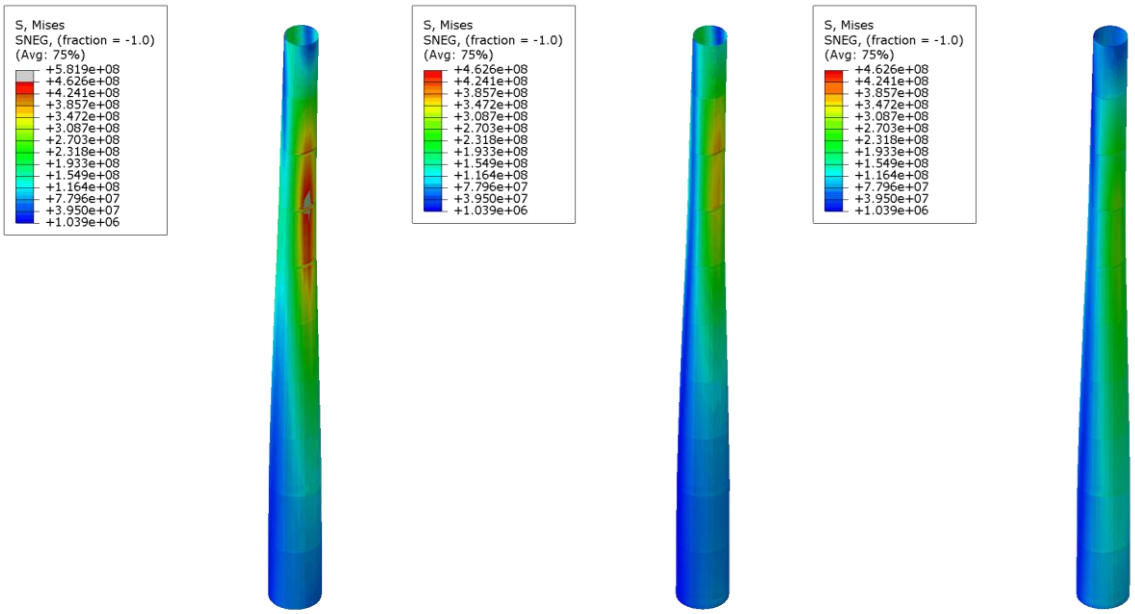

(a) (b) (c)

Figure 12: Von Mises stress contour map on the wind tower for: (a) Reference, (b) RD = 0.8 and (c) RD = 1.1.

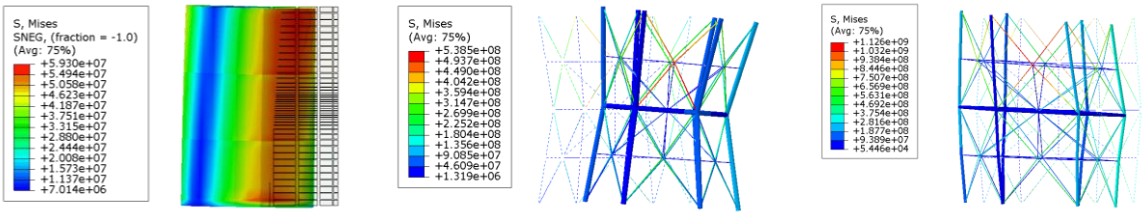

(a) (b) (c)

Figure 13: Von Mises stress contour map on the TP for: (a) Reference, (b) RD = 0.8 and (c) RD = 1.1.

	Reference	RD=0.8	RD=1.1	$\Delta\sigma = \frac{\sigma_{RD} - \sigma_{Reference}}{\sigma_{Reference}}$	
T10	270.25	279.48	188.78	3.41%	-30.15%
T9	465.18	440.72	289.13	-5.26%	-37.84%
T8	548.83	398.84	306.47	-27.33%	-44.16%
T7	518.75	366.79	293.72	-29.29%	-43.38%
T6	411.93	278.08	275.01	-32.49%	-33.24%
T5	297.83	244.47	231.97	-17.92%	-22.11%
T4	245.59	223.28	199.00	-9.08%	-18.97%
T3	199.96	195.48	180.17	-2.24%	-9.90%
T2	180.11	165.05	159.25	-8.36%	-11.58%
T1	189.29	184.52	161.81	-2.52%	-14.52%
TP	247.46	1128.89	2133.1	356.20%	762.02%
Monopile	273.45	233.26	189.32	-14.70%	-30.77%

Table 3. Maximum Von Mises stress of different segments in each case.

To verify the stress distribution, the same analyses are conducted through the 3D shell models. Stress contour maps corresponding to the time instant when the maximum tower stress occurs are shown in Figure 12. It can be seen that the reduction in peak stresses for the various cases decreases the risk of material yielding under extreme events. Stresses and scaled deformed shape for the traditional TP and novel HLS are shown in Figure 13; for RD = 0.8, the rocking mechanism expected by the Reduced Column Approach [10-11] is observed.

Table 3 reports that comparison of the maximum stresses for each segment of the tower and monopile. It can be seen that the novel HLS absorbed the peak stresses, as supposed, protecting the remaining tower and monopile. For the reference wind turbine, the highest stressed region occurs on the top half of the tower, which is vulnerable under combined loadings.

3.4 Seismic analysis

In addition to wind-seismic combined analysis, a seismic analysis is carried out for the reference wind turbine, HLS wind turbine with a reduction ratio of 0.5, 0.8 and 1.1, respectively. Dynamic response in terms of displacements, accelerations and bending moment envelopes is used to assess the beneficial impact of the HLS.

Figure 14 depicts the bending moment envelope profile of the complete wind turbine structure between the reference wind turbine and 3 cases of HLS wind turbine. For the RD = 1.1 case, global reduction can still be seen from monopile to tower, with 36% reduction at mudline and up to 37% in tower. The RD = 0.8 HLS wind turbine also exhibits improvement with a decrease of 28% of mudline bending moment and 30% in the central tower, while local bending-moment increment up to 7% exists on the top of the tower, similar to the wind-seismic combined case.

However, when RD = 0.5, the bending moment at mudline exceeds the result of the reference wind turbine with an increase of 11%. Besides, the response in the tower indicates negligible mitigation. This might be the reason that the optimization is performed based on combined wind-seismic analysis in which wind and seismic load coexist. It can be concluded that the participation of wind plays an important role in the dynamic response of HLS wind turbine with lower RD, while seismic action becomes more dominant for the higher RD case.

Figure 15 shows the displacement and acceleration at the top of the tower of each type of wind turbine. It can be concluded that the RD = 1.1 case results in the greatest reduction in terms of peak acceleration value, which is 29.28%, followed by 3.17% for the RD = 0.8 and -6.68% for the RD = 0.5 (negative means higher than the reference). Same to the bending-moment result, RD = 0.5 case exhibits negative effect in terms of vibration mitigation.

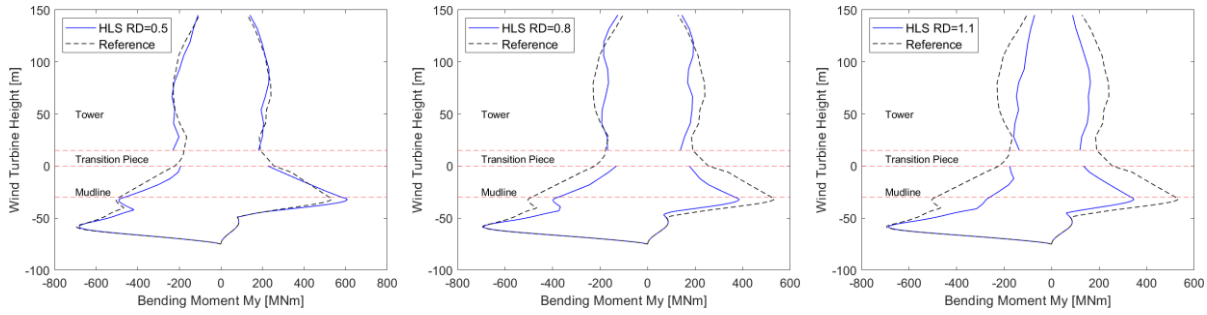

Figure 14: Bending moment envelope compared to the reference: (a) RD = 0.5, (b) RD = 0.8 and (c) RD = 1.1.

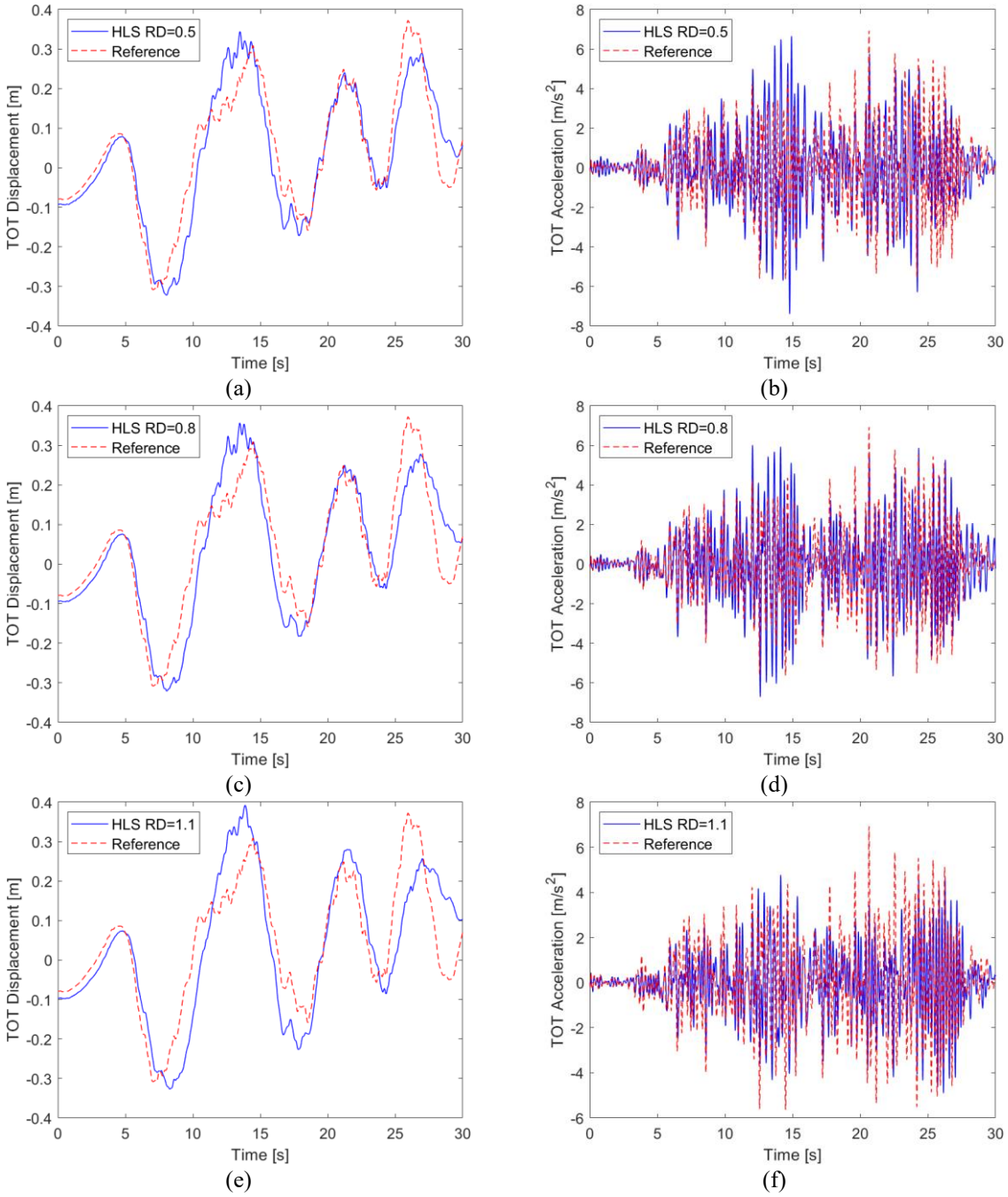

Figure 15: Displacement and acceleration time-history functions compared to the reference: (a, b) RD = 0.5, (c, d) RD = 0.8 and (e, f) RD = 1.1.

Figure 16 highlights locations of the maximum Von Mises stress in the tower for each type of wind turbine; it should be noted that the peak stresses occur along the side of the hub during the earthquake. Figure 17, on the other hand, depicts the stress distribution of different transition pieces at the same moment (deformation scaled up to 15 times), in which vague shapes and dashed lines denote undeformed shapes. Table 4 provides the maximum stress of all tower segments, transition piece (TP) and monopile, indicating that the HLS transition piece is densely stressed in comparison to the cylindrical shell transition piece and hence gives rise to the stress reduction in the tower during ground motion.

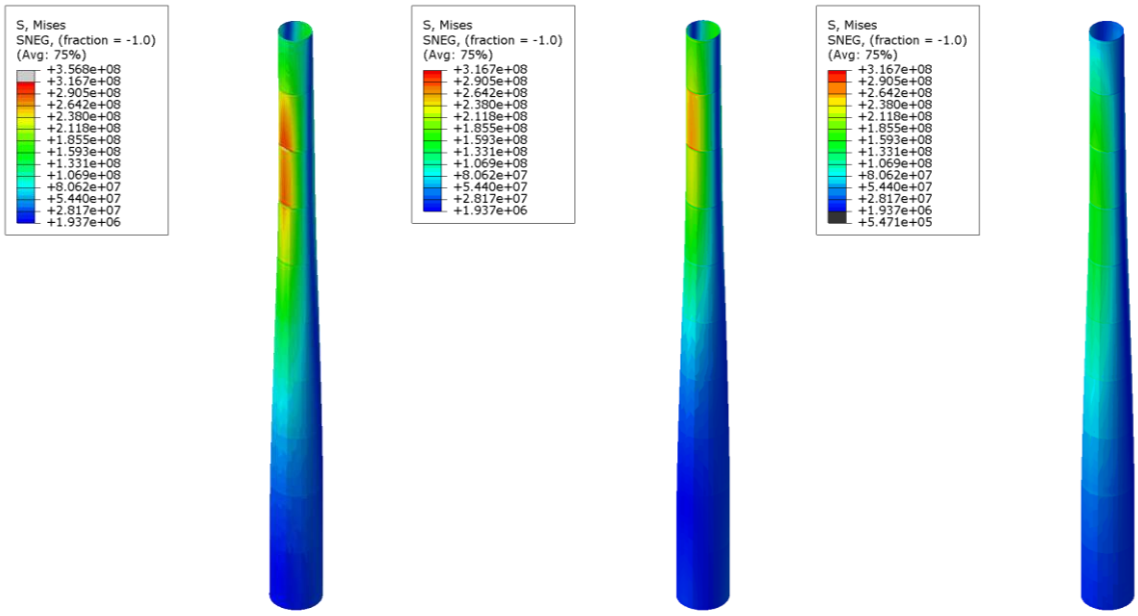

(a) (b) (c)

Figure 16: Von Mises stress contour map on the wind tower for: (a) Reference, (b) RD = 0.8 and (c) RD = 1.1.

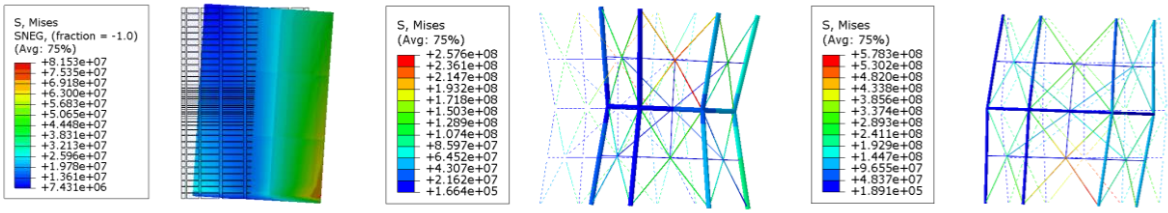

(a) (b) (c)

Figure 17: Von Mises stress contour map on the TP for: (a) Reference, (b) RD = 0.8 and (c) RD = 1.1.

	Reference	RD=0.8	RD=1.1	$\Delta\sigma = \frac{\sigma_{RD} - \sigma_{Reference}}{\sigma_{Reference}}$	
T10	225.78	246.81	158.02	9.31%	-30.01%
T9	337.68	299.68	195.65	-11.25%	-42.06%
T8	303.07	257.83	187.54	-14.93%	-38.12%
T7	279.83	216.79	177.57	-22.53%	-36.54%
T6	214.75	155.46	155.73	-27.61%	-27.49%
T5	167.29	124.42	122.20	-25.63%	-26.95%
T4	131.12	107.22	96.25	-18.23%	-26.60%
T3	98.82	90.70	82.06	-8.22%	-16.96%
T2	75.05	77.81	69.97	3.67%	-6.77%
T1	79.07	68.94	65.87	-12.81%	-16.70%
TP	113.29	431.73	1012.08	281.10%	793.39%
Monopile	159.77	150.38	150.14	-5.88%	-6.03%

Table 4. Maximum Mises stress of different segments in each case (MPa).

3.5 Concluding Remarks

In this study, a novel transition piece, called the Hourglass Lattice Structure is proposed. By adhering to the principles proposed for the Reduced Column Section approach [10-11], the HLS is able to mitigate the combined wind-seismic response of the wind turbines.

A numerical investigation on the IEA 15MW reference wind turbine [12] has been conducted. Three versions of the HLS defined by a reduction ratio RD of 0.5, 0.8 and 1.1 have been optimized and applied to the reference wind turbine model. The main results are:

- Although absolute tower displacements are increased, peak acceleration is reduced for every case.
- Maximum bending moment reduction up to 40% has been achieved.
- Stresses are largely reduced in both wind tower and monopile, decreasing the risk of material yielding under extreme events.

The conducted analysis is performed considering elastic properties. Future developments entail introducing plasticisation in selected elements of the HLS to increase energy dissipation, as well as incorporating seismic devices such as dampers or self-centring elements to enhance mitigation under both wind and seismic loadings.

ACKNOWLEDGMENTS

Dr. Tombari gratefully acknowledges the financial support of the UK Engineering and Physical Sciences Research Council (EPSRC) through the New Investigator Award (EP/W001071/2), titled “Structural Life Cycle Enhancement of Next-Generation Onshore and Offshore Wind Farms”.
Yucheng Peng acknowledges the financial support of the Chinese Scholarship Council (CSC).

REFERENCES

[1] GWEC, *Global Wind Report 2024*. Global Wind Energy Council, 2024.

[2] K. H. Jang and K. W. Ryu, Blade Design and Aerodynamic Performance Analysis of a 20 MW Wind Turbine for LCoE Reduction. *Energies*, **16**, 13, 2023, doi: 10.3390/en16135169.

[3] S. Bhattacharya *et al.*, Seismic design of offshore wind turbines: Good, bad and unknowns. *Energies*, **14**, 12, 2021, doi: 10.3390/en14123496.

[4] D. V. Ngo and D. H. Kim, Seismic responses of different types of offshore wind turbine support structures. *Ocean Engineering*, **297**, 117108, 2024, doi: 10.1016/j.oceaneng.2024.117108.

[5] L. A. Padrón, S. Carbonari, F. Dezi, M. Morici, J. D. R. Bordón, and G. Leoni, Seismic response of large offshore wind turbines on monopile foundations including dynamic soil–structure interaction. *Ocean Engineering*, **257**, 111653, 2022, doi: 10.1016/j.oceaneng.2022.111653.

[6] F. Liang, X. Jia, H. Zhang, C. Wang, and P. Shen, Seismic responses of offshore wind turbines based on a lumped parameter model subjected to complex marine loads at

scoured sites. *Ocean Engineering*, **297**, 116808, 2024, doi: 10.1016/j.oceaneng.2024.116808.

[7] Y. Lu *et al.*, Dynamic analysis of MTMD vibration reduction for offshore wind turbine under combined wind-wave-seismic loads. *Structures*, **72**, 108207, 2025, doi: 10.1016/j.istruc.2025.108207.

[8] Y. Gao *et al.*, Integrated design and real-world application of a tuned mass damper (TMD) with displacement constraints for large offshore monopile wind turbines. *Ocean Engineering*, **292**, 116568, 2024, doi: 10.1016/j.oceaneng.2023.116568.

[9] K. Ke, W. Xie, X. Zhou, Y. Wang, and X. He, A novel self-centring jacket-type offshore wind turbine structure: A proof-of-concept study and seismic fragility analysis. *Thin-Walled Structures*, **205**, 112407, 2024, doi: 10.1016/j.tws.2024.112407.

[10] R. Rostami and A. Tombari, A novel reduced column section approach for the seismic protection of wind turbines. *Engineering Structures*, **282**, 115807, 2023, doi: 10.1016/j.engstruct.2023.115807.

[11] A. Tombari and R. Rostami, A Novel Reduced Column Approach for the Mitigation of Earthquake-Induced Vibrations of Wind Turbines. in *Journal of Physics: Conference Series*, Institute of Physics, 2024, doi: 10.1088/1742-6596/2647/3/032004.

[12] E. Gaertner *et al.*, Definition of the IEA Wind 15-Megawatt Offshore Reference Wind Turbine Technical Report. 2020. [Online]. Available: www.nrel.gov/publications.

[13] M. Zhu, F. McKenna, and M. H. Scott, OpenSeesPy: Python library for the OpenSees finite element framework. *SoftwareX*, **7**, 6–11, 2018, doi: 10.1016/j.softx.2017.10.009.

[14] R. Storn and K. Price, Differential Evolution-A Simple and Efficient Heuristic for Global Optimization over Continuous Spaces. Journal of Global Optimization, **11**, 341-359, 1997, doi: 10.1023/A:1008202821328.

[15] ABAQUS. ABAQUS Analysis user's Manuals: Version 6.13. Providence, RI, USA: Dassault Systemes Simulia Corporation; 2013.